Development and Optimization of a Quantitative DNA Base Excision Assay

A Thesis

Submitted to the Faculty

of

Drexel University

by

Christopher Arif Abdullah

in partial fulfillment of the

requirements for the degree

of

Masters of Science in Biomedical Engineering

September 2008

Dedications

To my amazing family and friends.

The have provided me with the support and care necessary to be successful.

Acknowledgements

The success of this research would have not been possible without the direction and mentorship provided by Dr. Bahrad Sokhansanj. Also, Andrew Atkins, He Zhao, and Mike Lanewala, members of the Sokhansanj lab, have provided enormous amounts of insight and assistance into the work that I have done. I would also like to thank my defense committee members Dr. Andres Kriete and Dr. Chang Chang for their insight and suggestions

Table of Contents

List of Tables

List of Figures

Abstract

Development and Optimization of a Quantitative DNA Base Excision Assay
Christopher Abdullah

The base excision repair (BER) system routinely removes damaged bases from DNA to conserve the integrity of the genome. The aims of this study were to design and optimize an assay using fluorescent kinetic data from molecular beacon (MB) oligonucleotides to generate an enzymatic model of base excision. Damaged bases, including 8-oxo-7,8-dihydroguanine (8oxoG) and uracil, were incorporated within 5'-fluorescein, 3'-Dabcyl labeled stem-loop oligonucleotides for use in this repair assay. Fluorescence data was recorded to monitor the kinetics of the base excision. Parameters were estimated using nonlinear regression to characterize the efficiency of repair proteins in whole cell extracts. This assay provides a simple, reproducible, and quantitative method to determine BER efficiency as a means of characterizing DNA repair capacity in cells.

I. Introduction and Background

A. Base Excision Repair

Base excision repair (BER) includes several endogenous, evolutionarily conserved mechanisms that remove inappropriate bases that result from DNA damage, examples of which include oxidation, alkylation, and single strand breaks. Transcription of such bases leads to mutations that may subsequently cause various disease phenotypes. Specifically, DNA damage can occur via the action of genetic toxins such as reactive oxygen species (ROS). ROS, including radicals of O_2^-, OH, and H_2O_2, can be generated in vivo as by-products of cellular respiration in mitochondria, during ionizing radiation, and during oxidative metabolism (Hegde, Hazra et al. 2008). The connection between the presence of these ROS and the initiation and development of cancer has been documented (Boiteux and Radicella 2000; David, O'Shea et al. 2007).

Due to its low redox potential, the base guanine (G) becomes commonly oxidized by various ROS to 8-oxo-7,8-dihydroguanine (8oxoG), which pairs with a complementary adenine (A) to cause a GC→AT transversion in the DNA sequence (David, O'Shea et al. 2007; Hegde, Hazra et al. 2008). The BER pathway requires several types of enzymes to be present in order to reverse ROS-induced damage and oxidative stress. These enzymes include a DNA glycosylase, which excises the 8oxoG to create an AP (apurinic/apyrimidinic) site (representing AP lyase activity), an AP endonuclease, which cleaves the AP site to generate a 3'-OH and a 5'-deoxyribophosphate (dRp), a DNA polymerase, which inserts the correct, nicked base into the single nucleotide gap, and a DNA ligase, which seals the correct base into the sequence.

The structures of 8-oxoG and the hydrogen bonding interactions between normal and damaged base pairs are depicted below:

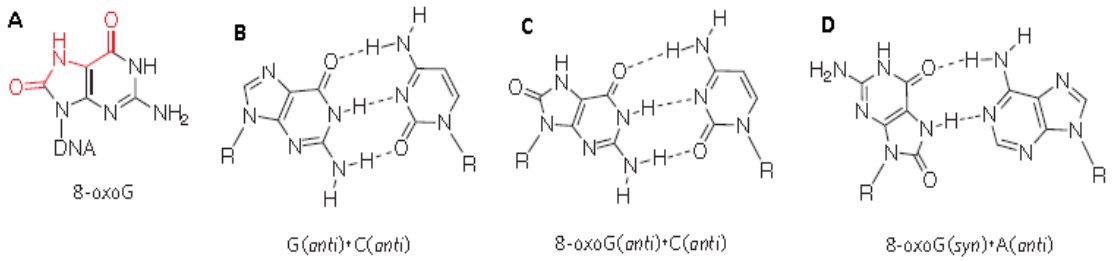

Figure 1 – The effect of 8oxoG on a normal guanine and cytosine base pairing causes a transversion mutation from a G:C pair to eventually an A:T pair. A: Structure of 8-oxoG reveals an extra carboxyl group. B: A typical, non-mutated pairing of guanine (G) with cytosine (C) involves three hydrogen bonds and an "anti-anti" conformation. C: 8oxoG can still correctly base pair with C in an "anti-anti" arrangement without mutation. D: However, once 8oxoG flips to a different conformation ("syn"), it will form two hydrogen bonds and base pair with the other purine (A), causing a mutation (Adapted from (David, O'Shea et al. 2007)).

The specific DNA glycosylase that is active in 8oxoG excision is 8-oxoguanine-DNA glycosylase/AP lyase (Ogg1). This particular enzyme is characterized by a relatively slow or weak AP lyase activity, meaning that it leaves an AP site intact (uncleaved) and occupies it (with a half-life of >2 hours). This rate-limiting action of OGG1 has been shown to be avoided in the presence of APE1, which releases Ogg1 from an AP site (after glycosylase activity), allowing it to explore further 8oxoG mismatches (Vidal, Hickson et al. 2001). The coordination of Ogg1 activity by APE1 was further demonstrated when equimolar concentrations of the two enzymes increased the glycosylase activity of Ogg1 4-5-fold and created Michaelis-Menten kinetics (Hill, Hazra et al. 2001). Although Ogg1 samples millions of base pairs per second, it has been established to maintain a 10^5-fold higher affinity for 8oxoG versus normal G, demonstrating its effectiveness in early BER steps (David, O'Shea et al. 2007). Specifically, Ogg1, by itself, leaves a 3'-phosphoglycolaldehyde (PUA) immediately before the gap created by the excised 8-oxoG and a 5'-phosphate (normal) immediately after the gap (Hegde, Hazra et al. 2008).

Ogg1 has been shown to have a high affinity for the AP site that it generates. Thus, Ogg1 essentially remains bound to the DNA halting the repair pathway. Ogg1 cannot repair other

damaged sites, and the DNA cannot proceed further through the pathway. APE1 and NEIL1 have been hypothesized to displace the Ogg1and each perform lyase activity which pushes the DNA through the repair pathway as well as freeing Ogg1 to search out other damaged bases.

APE1 (AP site-specific endonuclease 1) modifies the damaged DNA strand (Strauss, Beard et al. 1997) at the AP, or abasic, site to create a 3'-OH group before the gap and a 5'-dRp group after the gap, and these moieties can then properly connect a newly incorporated base to the existing strand via the intrinsic dRp lyase activity of mammalian Polβ (Hegde, Hazra et al. 2008). When active after Ogg1 activity (weak AP lyase), APE1 replaces the 3'-PUA with a 3'-OH (normal) to prepare the gapped DNA for Polβ activity.

Incorporation of uracil residues in DNA can be as problematic as 8oxoG damages. Uracil residues can result from deamination of a cytosine, which may cause CG→TA mutations. Base excision repair of uracil follows a similar pathway as that of 8oxoG. Uracil residues are excised by a uracil DNA glycosylase (UDG) leaving an AP site. APE1 then incises the phosphodiester backbone in preparation for a DNA polymerase to finish the repair pathway and restore the correct bases (Maksimenko, Ishchenko et al. 2004; Liu, Yang et al. 2007).

B. DNA Substrates

For use in this assay, two types of oligonucleotides were considered (Liu, Yang et al. 2007). Molecular beacons, purchased from Operon Technologies, are single stranded oligonucleotides which upon annealing conform to a stem-loop structure. At the 5' end of the strand, a fluorescein was attached whereas at the 3' end of the DNA strand a Dabcyl quencher was attached. Using fluorescence energy transfer (FRET) technology, the probes when in closed conformation do not fluoresce due to the close proximity of the fluorescein and the quencher. Sequences of 39 base pairs (bp) were selected as previously described (Maksimenko, Ishchenko

et al. 2004) and can be found in Table 1. The stem and loop portions of the MB each consisted of 13 bps. Two control strands were used. FL35 was a positive control with no damage or quencher. The negative control was FD35 which lacked damaged bases but contains both the fluorophore and quencher. The FDU MB contained multiple uracil residues throughout the stem and loop. FDAPE1 and FD8oxoGC contained single residues of either uracil or 8oxoG, respectively, at position 7 in the stem. Removal of the base from this position has previously been shown to destabilize the stem (Malins, Polissar et al. 2000) and separate the fluorophore and quencher causing increased fluorescence (Maksimenko, Ishchenko et al. 2004). Complementary single-stranded 13 base pair (bp) strands were designed and also ordered from Operon Technologies. The sequences are listed in Table 2. Again, damage was placed at position 7 in these strands so that excision of the base would destabilize the oligonucleotide.

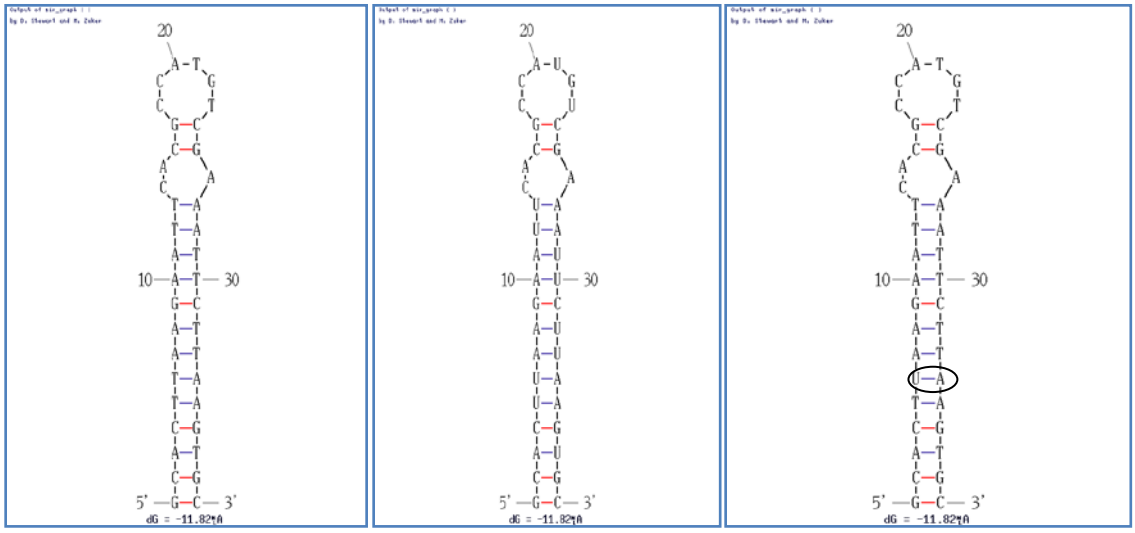

Figure 2-Oligonucleotide conformations. The left panel depicts the FL35 (5'-FITC) and FD35 (5'-FITC, 3'Dabcyl) structures. The center panel shows the FDU oligo (5'-FITC, 3'Dabcyl). The right panel shows the FDAPE1(5'-FITC, 3'Dabcyl) structure. Also, the FD8oxoGC conformation is the same as the FDAPE1, but with an 8oxoG paired across from a C in the circled position (Dinamelt 2008. http://dinamelt.bioinfo.rpi.edu).

Table 1-Molecular beacon sequences

Oligonucleotide	Sequence
FL35	[FITC]GCACTTAAGAATTCACGCCATGTCGAAATTCTTAAGTGC
FD35	[FITC]GCACTTAAGAATTCACGCCATGTCGAAATTCTTAAGTGC[Dabcyl]
FDU	[FITC]GCACUUAAGAAUUCACGCCAUGUCGAAAUUCUUAAGUGC[Dabcyl]
FDAPE1	[FITC]GCACTUAAGAATTCACGCCATGTCGAAATTCTTAAGTGC[Dabcyl]
FD8oxoGC	[FITC]GCACT[8oxoG]AAGAATTCACGCCATGTCGAAATTCTTCAGTGC[Dabcyl]

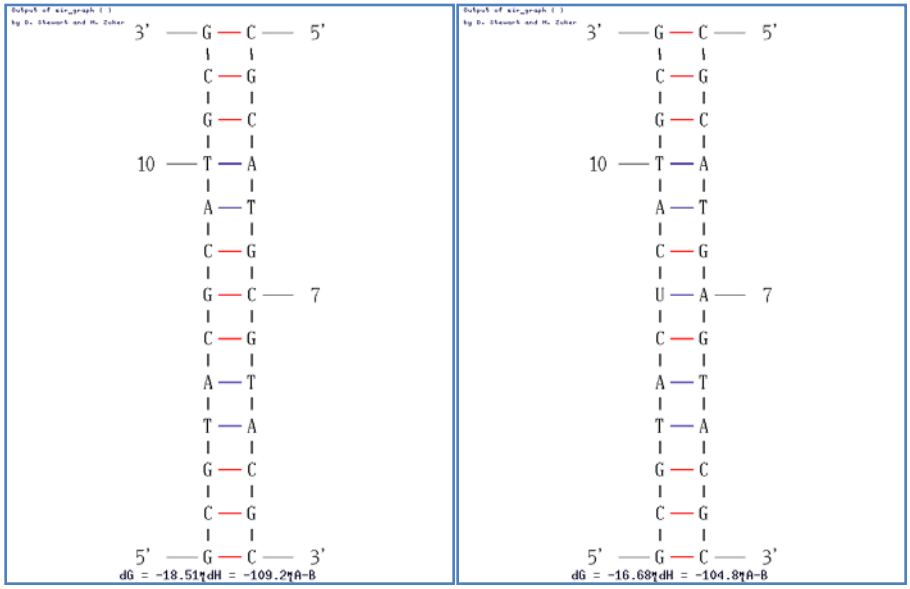

Figure 3-Oligonucleotide conformations for the double stranded probes. The left panel represents the F-cont-D-ssC or F-8oxoG-D-ssC (if the G at position 7 is replaced by an 8oxoG. The right panel represents the F-U-D-ssA combinations. The fluorescent molecule is attached to the damaged portion of the probe. (Dinamelt 2008. http://dinamelt.bioinfo.rpi.edu)

Table 2-Single strand oligonucleotides for hybridization to create double stranded oligonucleotide probes

Oligonucleotide	Sequence
F-cont	[FITC]GCGTACGCATGCG
F-8oxoG	[FITC]GCGTAC[8oxoG]CATGCG
F-U	[FITC]GCGTACUCATGCG
D-ssA	CGCATGAGTACGC[Dabcyl]
D-ssC	CGCATGCGTACGC[Dabcyl]

This project intends to improve upon current methods of measuring base excision kinetics. Common methods currently being used include radioactive labeling, gel electrophoresis, and autoradiography (Krokan and Wittwer 1981; Tchou, Kasai et al. 1991; Ischenko and Saparbaev 2002). Each of these methods is time consuming with indirect assaying via separation techniques. The proposed assay proposes several means of simplifying the detection of base excision as well as to allow real-time quantification. Fluorescence measurements provide a much simpler means of assaying activity over radioactive tags. This assay also hopes to improve reaction conditions to support whole cell extracts from different sources as well as provide a real-time assay for detection of base excision kinetics. This assay also should improve upon the number of cells required for lysate extraction. Previously between 5×10^7 and 5×10^9 cells have been required for cell extracts to provide enough protein for a reproducible assay (Smeaton, Miller et al. 2007). Lastly, kinetic parameters can be estimated from this data to give a quantitative representation of the efficiency in extracts from different populations of cells.

II. Specific Aims

The overall objective of this project was to develop and optimize a protocol for assaying base excision kinetics in whole cell lysates. Using FRET-based technology with oligonucleotides containing damaged bases, a simple method for assessing base excision efficiency in different cell populations.

A. Probe Validation

An appropriate FRET probe must be selected according to several criteria. The fluorescent probe should have a high efficiency of quenching. The probe must be stable in the reaction buffer once quenched. Purified recombinant base excision proteins should be able to remove the damaged bases and increase fluorescence. Double stranded probes and single stranded probes should each be tested and one selected for further use in the assay.

B. Reaction Optimization

Several types of base damage are being observed, and the proteins associated with the removal of these damages require different buffer conditions. A single whole cell extract buffer should be selected to meet the following conditions. Ability to observe positive signals for removal of each of the damages described (uracil and 8oxoG). Minimal nonspecific nuclease activity should be detected. Buffer components should not interfere with fluorescent probes.

C. Reproducibility of Assay

With probes and buffers optimized, the protocol for a base excision assay needs to be reproducible in several ways. The assay should provide consistent results from within extracts from the same preparation as well as across preparations made on different days. Also, this assay should provide results using a small scale extract protocol to minimize the necessary cell count.

D. Kinetic Parameter Estimation

With the reproducible results, an enzymatic model should be fit to the fluorescent data to provide kinetic parameters. A least squares method nonlinear regression fit can be used to generate the parameters. These parameters then can be used to describe a cell population's efficiency of base excision. Base excision efficiency then could be compared across cell populations.

III. Methods

Initial conditions for the molecular beacon assay were performed using the protocol used by Ischenko (Ischenko and Saparbaev 2002) for the whole cell extract buffer. The lysis protocol was adapted from another group doing work with Ogg1 assay development (Paz-Elizur, Elinger et al. 2007). A more thorough discussion of the optimization of this buffer as well as other conditions of the molecular beacon assay is provided in the Results section.

A. Cell Culture

All cells were grown at 90% humidity under 5% CO2 at 37C. Jurkat medium consisted of RPMI supplemented with 10 mM HEPES (pH 8.0), 1 mM sodium-pyruvate, 10% FBS, 2mM L-glutamine, gentamycin, glucose.

B. Whole Cell Lysate Extraction

Cells were pelleted by centrifugation at 250xg for 10 minutes. The medium was removed, careful not to disrupt the pellet. Cells were resuspended in phosphate buffered saline (PBS), counted using a hemocytometer, and diluted to 10^6 cells per ml. 50 ul of lysis buffer (50 mM HEPES (pH 8.0), 10 mM EDTA, 0.5 M KCl, 0.1% Tween-20, 5% glycerol) per 10^6 cells were then added to the pellet The pellet was then vortexed until the solution became cloudy with cell debris. The lysate was then centrifuged at 15000xg at 4C for 15 minutes. The supernatant was then removed and protein levels quantified. Aliquots were then stored at -20C for later use.

C. Molecular Beacon Assay

Reactions were performed in a 96-well black-wall, round-bottom plate. The standard assay consisted of 100 nM of each specified molecular beacon oligonucleotides in 100 ul of reaction buffer (20 mM HEPES pH 7.5, 50 mM KCl, 5 mM EDTA, 20 mM $MgCl_2$, 1 mM beta-mercaptoethanol, 0.1 mg/ml BSA). To ensure hybridization, samples were heated to 90C for 3 minutes and allowed to cool slowly to room temperature for 15 minutes. The samples were then centrifuged at 7000xg for 3 minutes. After samples were added to plate, 50 ul whole cell extracts were added to each sample. Fluorescence was measured at 37C at an excitation wavelength of 488 nm and emission wavelength at 520 nm using a TECAN M200 platereader using the optimal gain settings in the iControl software program.

D. Double Stranded Oligonucleotide Assay

The double stranded assay was performed under similar conditions to the molecular beacon assay adapted from previous double stranded oligonucleotide assays. 50 pmol of each complementary oligonucleotide were suspended into 100 ul of reaction buffer (20 mM HEPES pH 7.5, 50 mM KCl, 5 mM EDTA, 20 mM $MgCl_2$, 1 mM beta-mercaptoethanol, 0.1 mg/ml BSA). Reaction mixtures then were heated to 90C for 3 minutes and cooled for 15 minutes to ensure hybridization. Samples were then centrifuged at 7000xg for 3 minutes and then plated into 96 well plates. Enzymes or cell extracts were then added and incubated at 37C. Fluorescence was measured at 37C with an excitation wavelength of 488 nm and emission wavelength of 520 nm using a TECAN M200 platereader using its optimal gain setting in the iControl software program..

IV. Results and Discussion

A. Double Stranded vs. Single Stranded Oligonucleotides

Initial studies were performed on the double stranded (ds) oligonucleotides to determine which oligonucleotide provided the best means to assay the base excision. Each of the single stranded oligonucleotides was incubated alone in Ogg1 reaction buffer (New England Biolabs). As seen in Figure 3, the oligos with Dabcyl alone show no fluorescence while F-cont and F-8oxoG show fairly different levels of fluorescence without the presence of any quenchers.

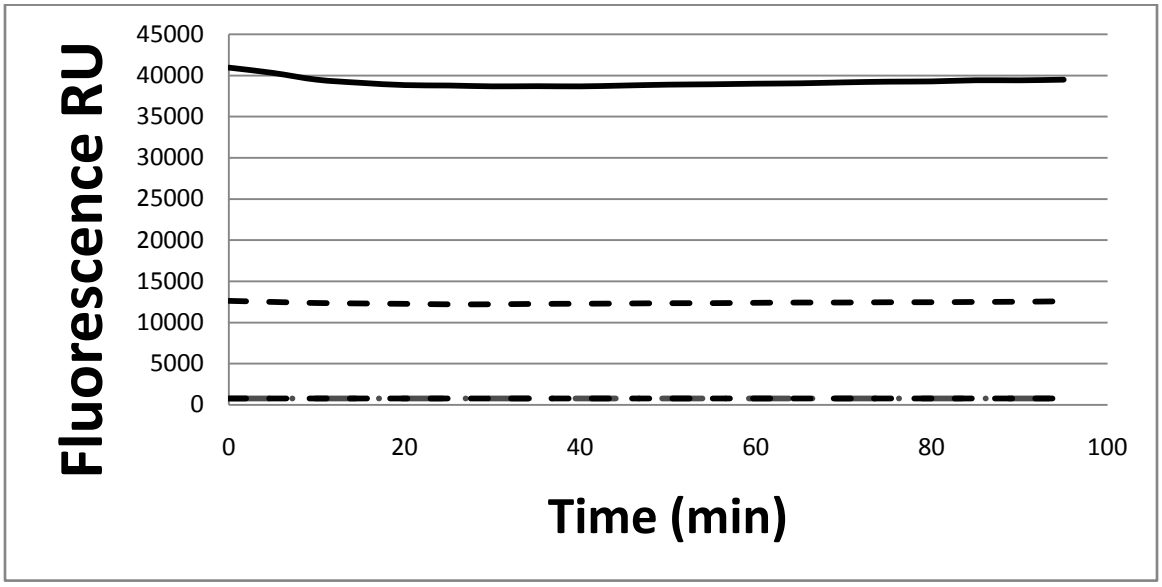

Figure 4-Fluorescence of single stranded oligonucleotides in reaction buffer. The two quencher complements, D-ssA (dashed gray) and D-ssC (dotted black) show no fluorescence. The two fluorescent complements, F-control (solid black) and F-8oxoG (dashed black) show considerably different levels of fluorescence at same concentrations at 500 nM.

Purified human Ogg1 and APE1 were incubated with 2 control strands containing both correct sequence complements as well as a mismatched bp at position 7. Neither strand showed any increase in fluorescence when incubated with the enzymes (Figure 4). Similarly, ds oligos

containing 8oxoG opposite to either cytosine or adenine were incubated with Ogg1 and APE1. Increased fluorescence indicates that the enzymes removed the 8oxoG paired with the cytosine, but not paired with the adenine. Ogg1 has a higher affinity for 8oxoG paired with cytosine as well as a higher removal rate. As previously discussed, the F-8oxoG substrate saturation occurs approximately near basal quenched levels of the controls.

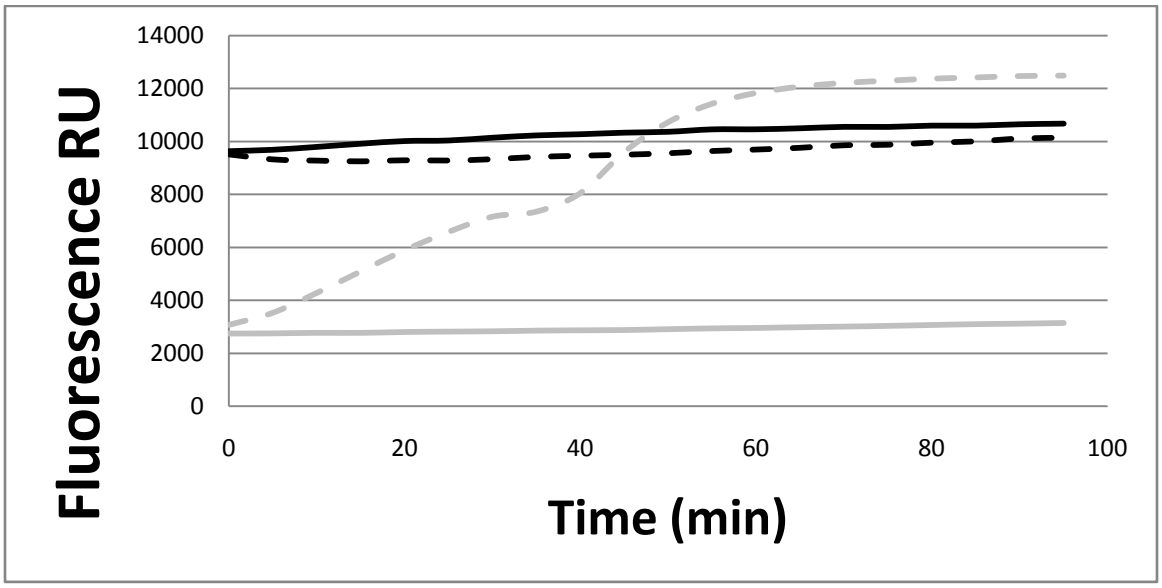

Figure 5-Hybridized Double stranded oligonucleotides were incubated with Ogg1 + APE1 with two different complements. Quenched fluorescent controls, F-cont-D-ssA (solid black) and F-cont-D-ssC (dashed black) show very little activity when incubated with enzymes. F-8oxoG-D-ssC (dashed gray) shows increased activity, but complete fluorescence occurs where the control oligonucleotides are completely quenched. F-8oxoG-D-ssA (solid gray) shows minimal activity indicated the specificity of Ogg1 to a C complement to 8oxoG.

Similar experiments with enzymes necessary for removal of uracil (UDG and APE1) were performed on the ds oligos in appropriate buffers (New England Biolabs). Figure 5 shows incubation of F-U-D-ssA with each enzyme individually as well as combined. APE1 alone caused no increase as expected because APE1 has no glycosylase activity. UDG incubation caused slight fluorescence increase which can be attributed to some destabilization of the ds oligo due to removal of the base alone. The highest increase was observed with both UDG and APE1. Under

these conditions, the combination of UDG uracil excision and APE1 nicking of the strand caused the large increase in fluorescence.

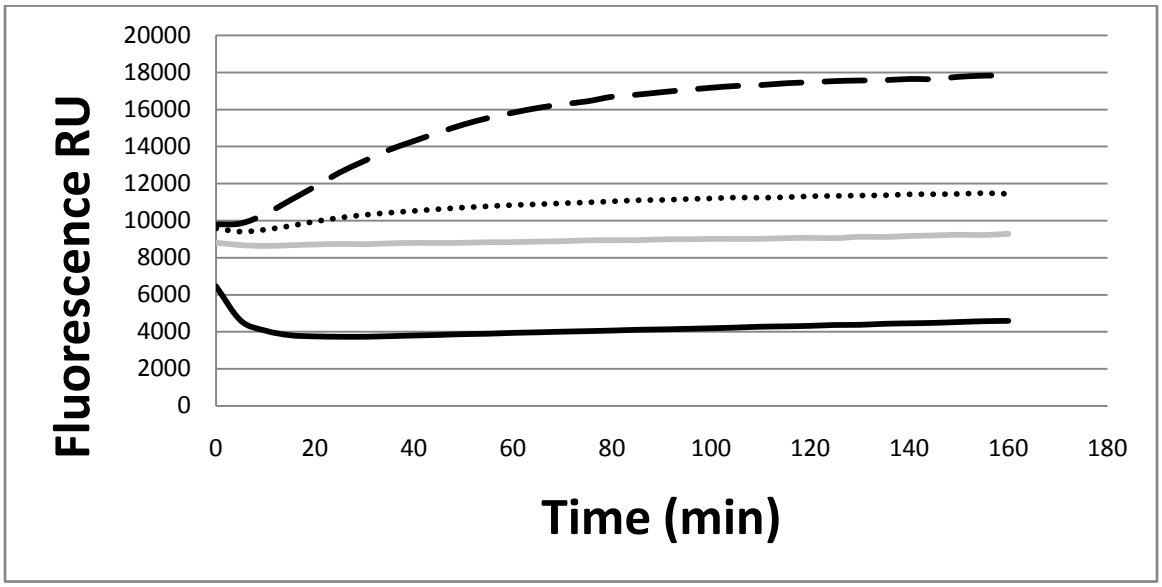

Figure 6- F-U-D-ssA double stranded oligonucleotides were incubated with either buffer only (solid black), APE1 only (solid gray), UDG only (dotted black), or UDG + APE1 (dashed black). UDG removal of uracil can be seen on the oligo, but APE1 addition further destabilizes the oligo which results in increased fluorescence.

Purified enzymes were incubated with the MB under the same conditions as the ds oligos. Similar to the F-U-D-ssA oligo, FDU (Figure 6) showed no increase with APE1, slight increase with UDG, and a much higher increase with both enzymes. The UDG alone has a more noticeable effect on the FDU due to multiple uracil residues unlike the ds oligo. Also important to note is the much larger separation between the quenched and fluorescing MB providing a much clearer positive result.

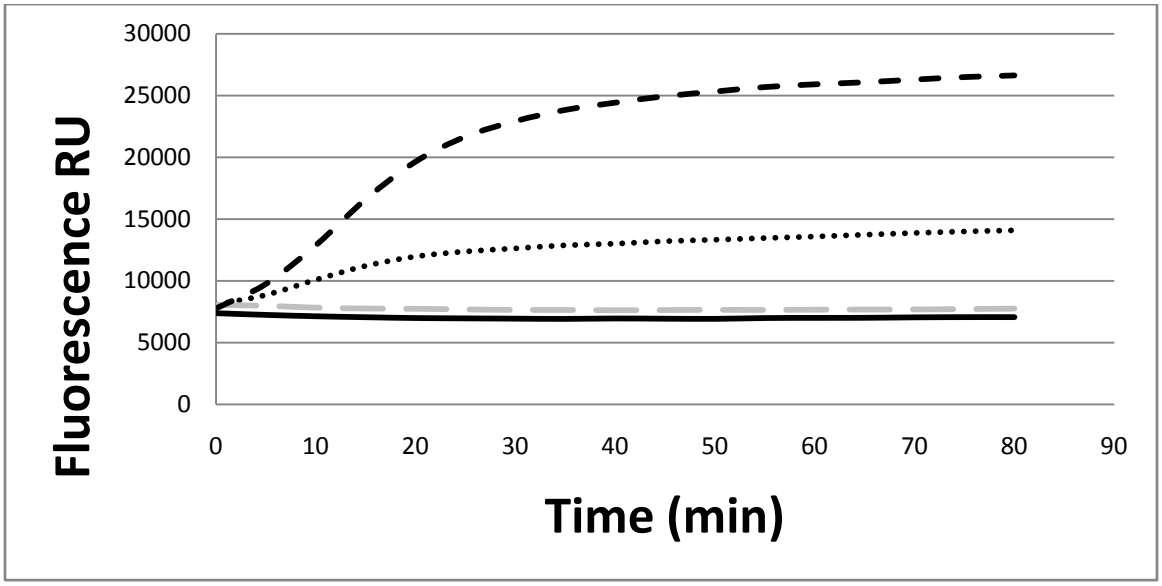

Figure 7- Enzymatic assay of FDU when incubated with Buffer Only (solid black), UDG (dotted black), APE1 (dashed gray), and UDG + APE1 (dashed black). Activity is only observed with co-incubation due to both the removal of the base as well as incision of the backbone.

The single uracil residue in the FDAPE1 MB provided the clearest picture as to the mechanism of the increased fluorescence. No increase is observed with single incubation of either UDG or APE1. But upon incubation with both, there is a dramatic increase in fluorescence. This suggested that removal of the uracil by UDG does not destabilize the MB enough to increase fluorescence. APE1 nicking of the strand does create a situation where the MB fluorescence increases.

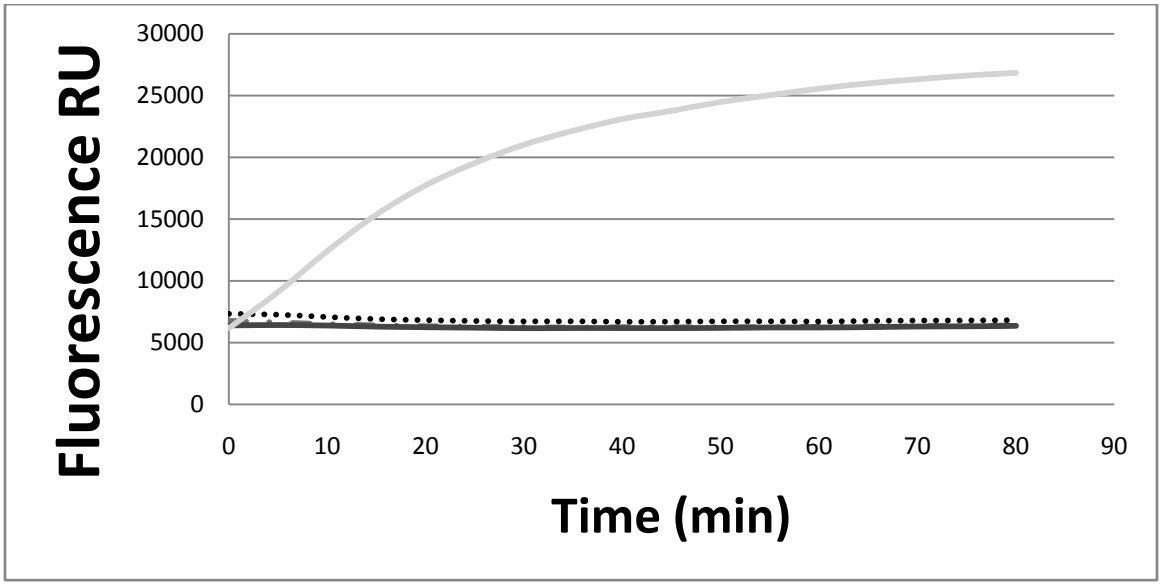

Figure 8-Enzymatic assay of FDAPE1 when incubated with UDG (solid black), APE1 (dotted black), and UDG + APE1 (solid gray). Activity is only observed with co-incubation due to both the removal of the base as well as incision of the backbone.

Additional experiments with a small molecule uracil glycosylase inhibitor (UGI) were performed for more perspective into the actual mechanism of the increased fluorescence due to enzymatic activity. The FDU and FDAPE1 MBs were each incubated in NEB APE1 buffer, and each reacted with UDG first. The FDU showed a low rate of increased fluorescence while the FDAPE1 showed no increase at all. The UGI was then added to the same samples and incubated at 37C. As seen in the middle panel of Figure 8, no increase in fluorescence can be seen from either MB. Lastly, APE1 addition caused increased fluorescence in both the FDAPE1 and FDU MBs. From this experiment, single base removal alone cannot cause an increase in the fluorescence. With UDG removing multiple uracil residues from the MB, destabilization allows for separation of the fluorophore/quencher pair and a small increase can be seen. With single damaged bases placed at the middle position in the MB's stem, base removal is not enough to cause increased fluorescence. APE1 nicking of the strand, therefore, caused the fluorescence increase.

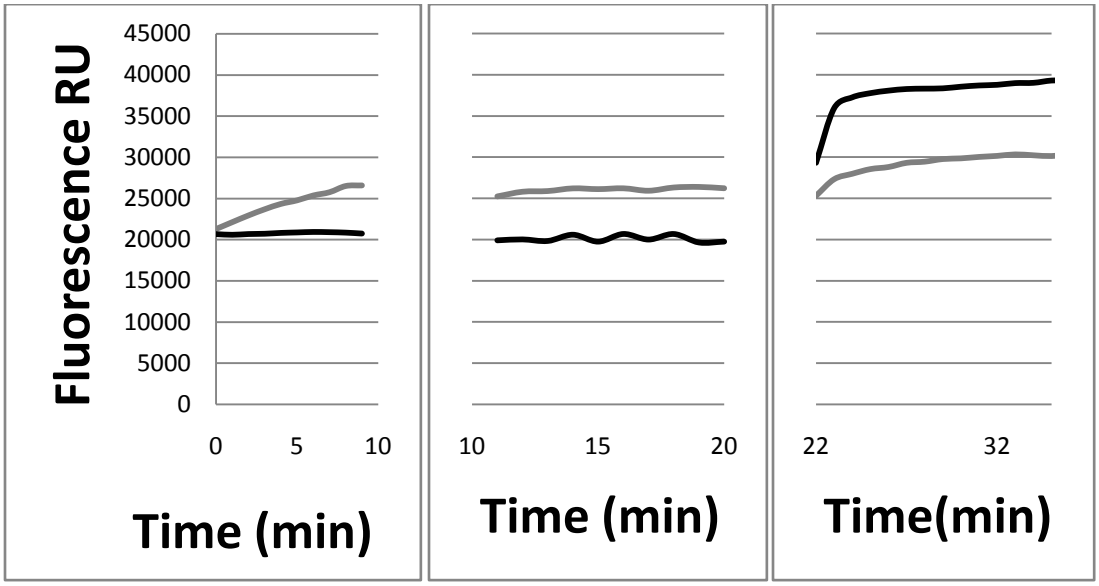

Figure 9- Time series addition of enzymes to FDU(solid gray) and FDAPE1 (solid black). UDG addition shows increase fluorescence in FDU, but not FDAPE1. Addition of UGI suspends the activity of UDG. Addition of APE1 increases the fluorescence of both FDU and FDAPE1 suggesting that APE1 nicking activity generates the separation of the fluorophore/quencher pair.

The FD8oxoGC pairs the 8oxoG with a cytosine and required the APE1 buffer (New England Biolabs) for any appreciable fluorescence increases to be observed. Because Ogg1 has both a glycosylase activity as well as AP endonuclease activity, there is always some increase in the FD8oxoGC when incubated with Ogg1. As seen in Figure 9, incubation with APE1 has no increase on fluorescence levels over incubation in buffer alone. Ogg1 alone does increase the fluorescence somewhat from basal levels. Incubation with Ogg1 and APE1 has a much higher fluorescence increase. This data also suggested an enhancement of Ogg1 turnover in the presence of APE1 (Hill, Hazra et al. 2001; Vidal, Hickson et al. 2001; Sidorenko, Nevinsky et al. 2007) as has been previously studied.

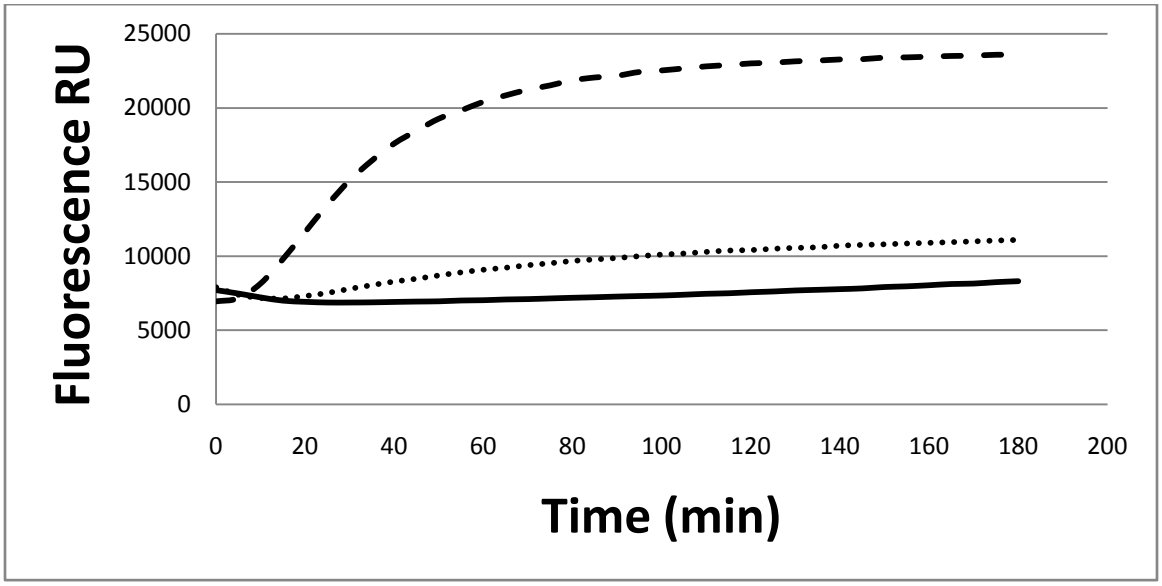

Figure 10-Enzymatic assay of FD8oxoGC when incubated with: Buffer (solid black), Ape1 (solid gray), Ogg1 (dotted black), and Ogg1 +APE1 (dashed black).

B. Reaction Optimization

EDTA and Magnesium

EDTA had previously been shown to decrease nonspecific activity via chelation of zinc ions required in the zinc-finger nucleases (Kreklau, Limp-Foster et al. 2001; Nyborg and Peersen 2004). Several concentrations of EDTA were used in buffers containing FDAPE1 to observe effects of EDTA on enzymes of interest. As seen in Figure 10, with increasing levels of EDTA in the buffer and constant protein levels, activity decreased significantly at concentrations as low as 2 mM. In addition to sequestering zinc ions, EDTA also binds magnesium ions which are required for APE1 activity. APE1 activity was diminished greatly without magnesium, and fluorescence increases were affected because of the decrease in APE1 AP endonuclease activity. To regain APE1 activity, several combinations of $MgCl_2$ and EDTA concentrations were performed. Previously, concentrations near 5 mM EDTA had shown no nonspecific nuclease

activity (Liu, Yang et al. 2007). As seen in Figure 11, 10 mM $MgCl_2$ with 5 mM EDTA restores the increase in fluorescence.

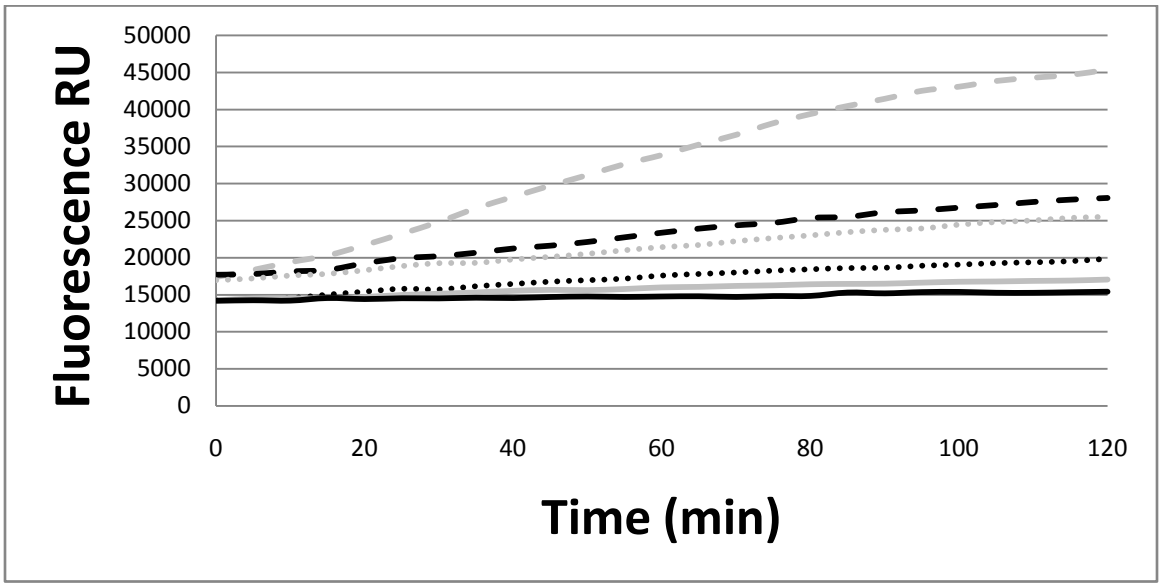

Figure 11-FDAPE1 incubation with 50 ug Jurkat extracts in cell extract buffer with increasing levels of EDTA. 0 mM (dashed black), 2 mM (dashed black), 5 mM (dotted gray), 10 mM (dotted black), 25 mM (solid gray), 50 mM (solid black). Fluorescence increases decrease with increasing levels of EDTA.

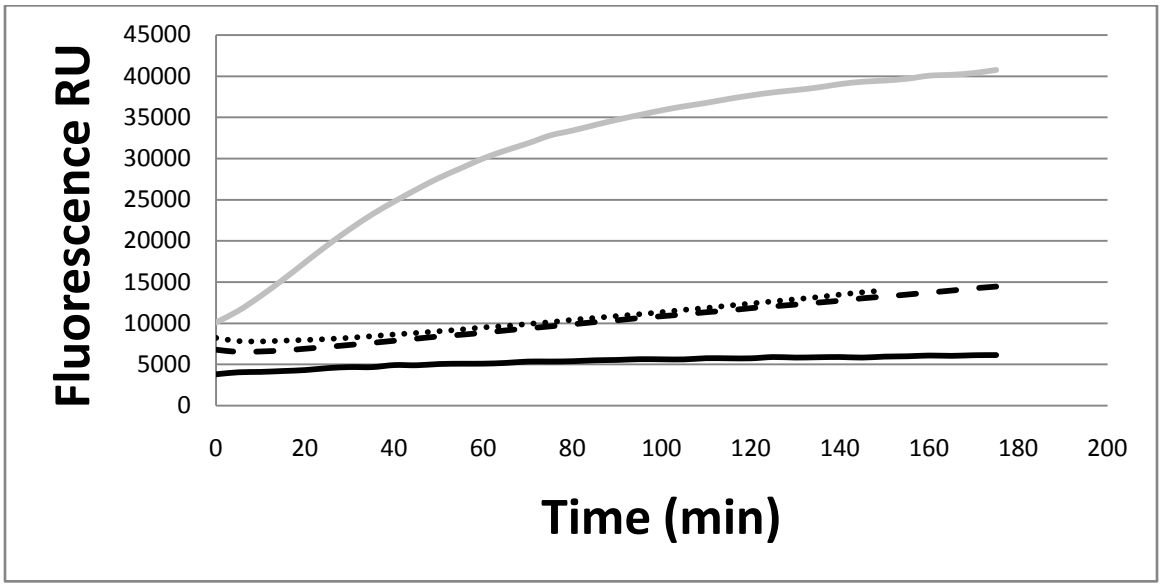

Figure 12- FDAPE1 incubated with 50 ug Jurkat extracts with different cominations of EDTA and MgCl2 concentrations. Solid black (10 mM EDTA + 10 mM MgCl2), solid gray (5 mM EDTA + 10 mM MgCl2), dotted black (5 mM EDTA), dashed black (10 mM EDTA).

Cell Optimization

With the reaction conditions optimized, several cell types were chosen and extracts used to validate the assay on different cell types. Figure 12, Figure 13, and Figure 14 show results from Jurkat, A549, and HEK293t cells respectively. Increases in fluorescence of each of the MBs containing damaged bases can be seen in all three of the cell lines. Also, differences in the efficiencies of the base removal can also be seen. From this data, the Jurkat cell line was chosen for the remaining experiments. The cell line had clear fluorescence increases in all of the damage-containing MBs. Because the Jurkat cell line is a suspension cell line, it was also preferred because any possible damaging effects of detaching adherent cells using trypsin could be avoided.

With the selection of the Jurkat cell line, protein quantification of the extracts was performed to determine the number of total cells which were required for individual reactions. The lysis protocol used one million cells per 50 ul of lysis buffer and observed protein concentrations can be seen in Figure 15. This protocol consistently provided adequate protein to use 30 ug of protein per reaction. Thus, this assay can be consistently performed using small scale extracts of one million cells per reaction which is lower than some previously described methods (Smeaton, Miller et al. 2007).

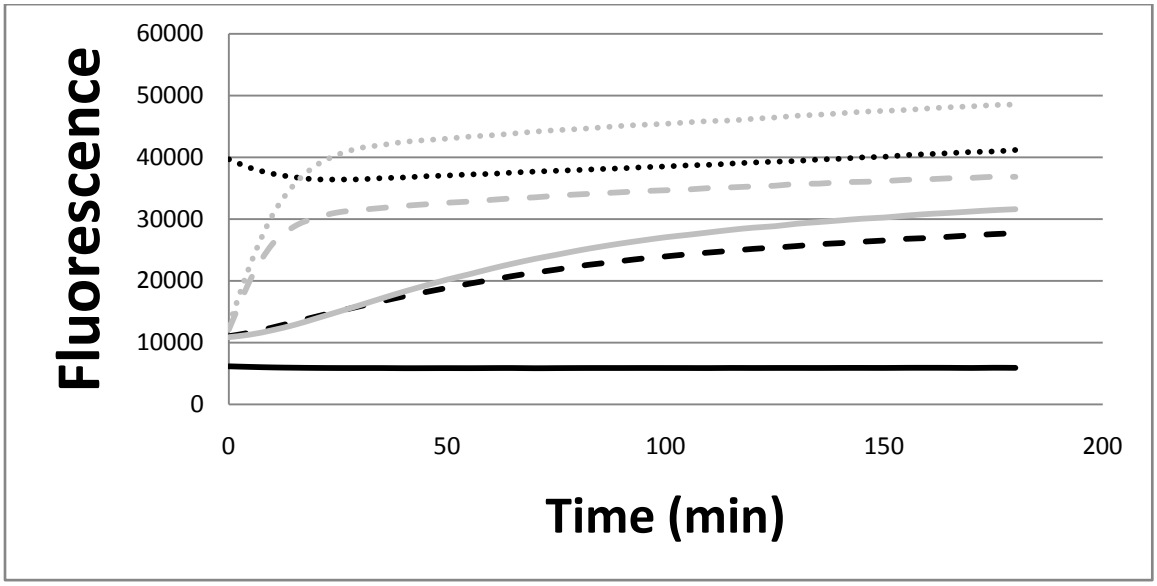

Figure 13- The standard molecular beacon assay protocol was followed with 100 ug Jurkat extracts for each species of MB as follows: Buffer (solid black), FL35 (dotted black), FD35 (dashed black), FD8oxoGC (solid gray), FDAPE1 (dotted gray), and FDU (dashed gray).

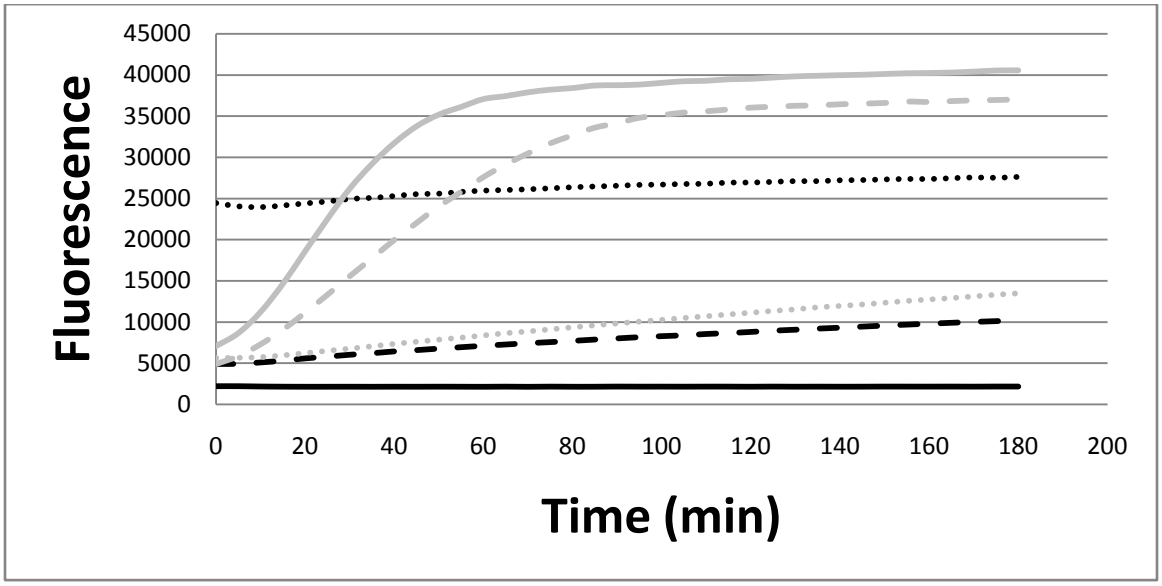

Figure 14- The standard molecular beacon assay protocol was followed with 100 ug A549 extracts for each species of MB as follows: Buffer (solid black), FL35 (dotted black), FD35 (dashed black), FD8oxoGC (dotted gray), FDAPE1 (dashed gray), and FDU (solid gray).

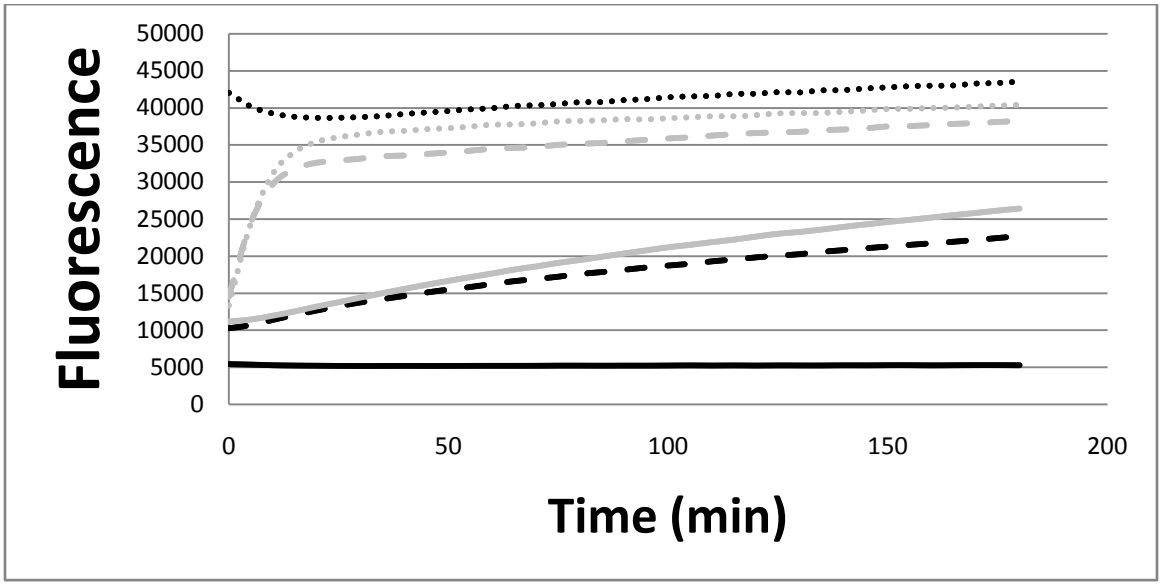

Figure 15-The standard molecular beacon assay protocol was followed with 100 ug HEK293 extracts for each species of MB as follows: Buffer (solid black), FL35 (dotted black), FD35 (dashed black), FD8oxoGC (solid gray), FDAPE1 (dotted gray), and FDU (dashed gray).

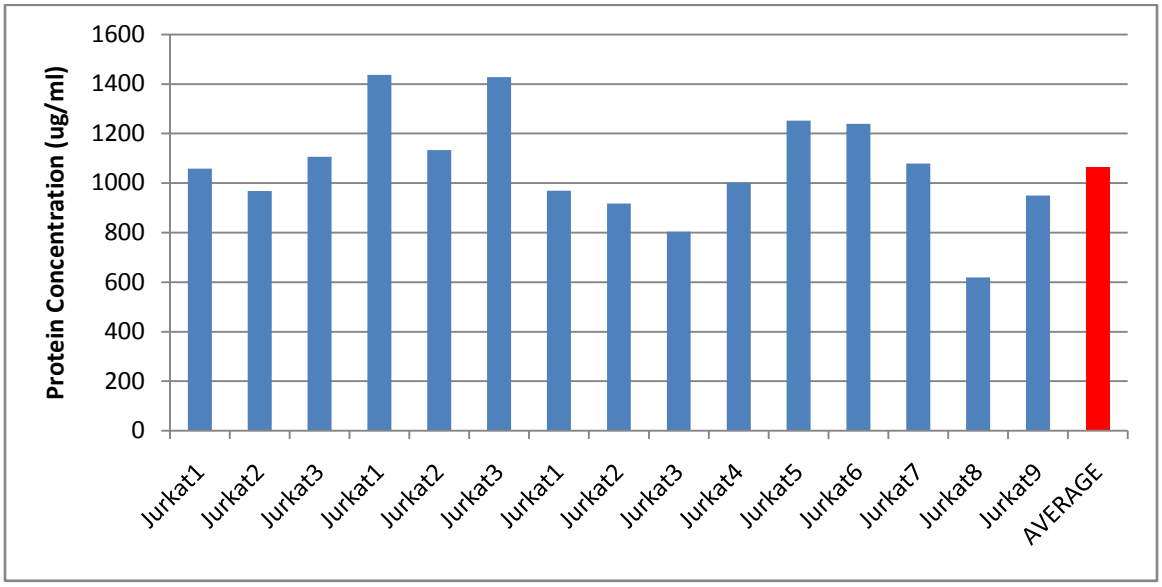

Figure 16-BCA protein quantification yields for 15 samples taken on 5 different days with 3 samples in parallel preparations

C. Reproducibility

Substrate Dilutions

Once the lysis protocol and reaction buffer were optimized, the molecular beacon assay was performed on each of the substrates with 30 ug whole cell extracts on differing concentrations of substrate. Initial reactions of varying concentrations of a single substrate were performed on separate plates. Because the platereader being used optimizes fluorescence to the highest fluorescence on the plate, lower concentrations of substrate had large variations because of the small dynamic range of the fluorescent signal. Figure 16,Figure 17, and Figure 18 show some of these results. For this reason, one substrate concentration with each of the MB in parallel was run so that the dynamic range was increased and allowed for a more reproducible analysis (Figure 19 and Figure 20). Additional considerations needed to be taken to adjust the fluorescence levels to account for the different substrate concentrations because the raw data output essentially was the same because of the optimal gain settings on the platereader. Substrate concentrations used for generation of kinetic curves were 100 nM, 250 nM, 500 nM, 750 nM, 1 uM, 1.25 uM, and 1.5 uM. Each MB reaction was performed in quadruplicate using whole cell extracts prepared in parallel.

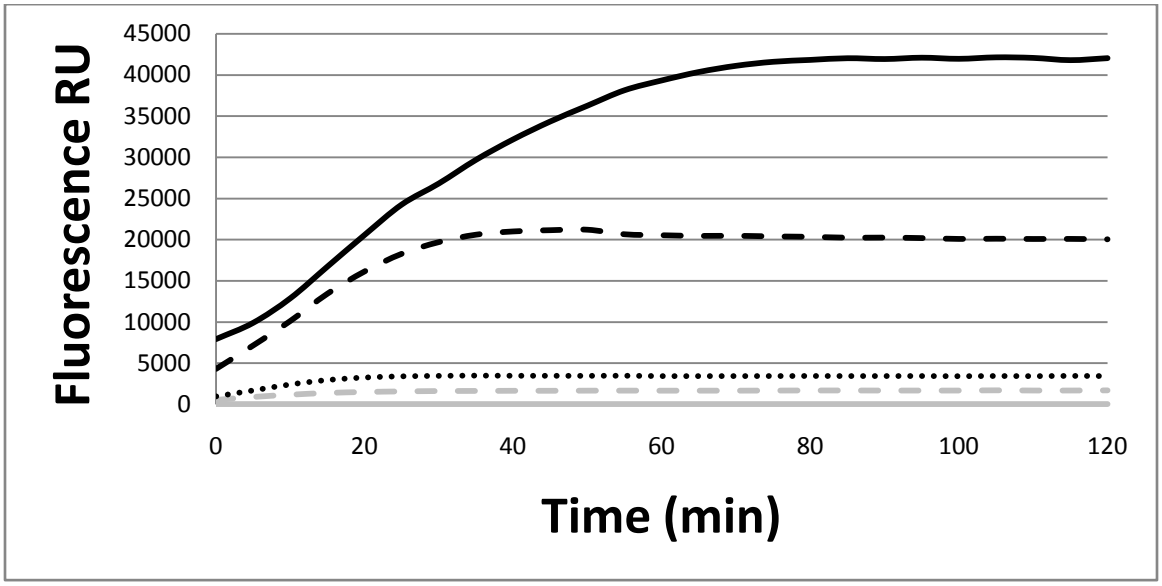

Figure 17-Standard FDAPE1 assay with 20 ug Jurkat extracts per reaction at different substrate concentrations: 50 nM (dashed gray), 100 nM (dotted black), 500 nM (dashed black), 1 uM (solid black

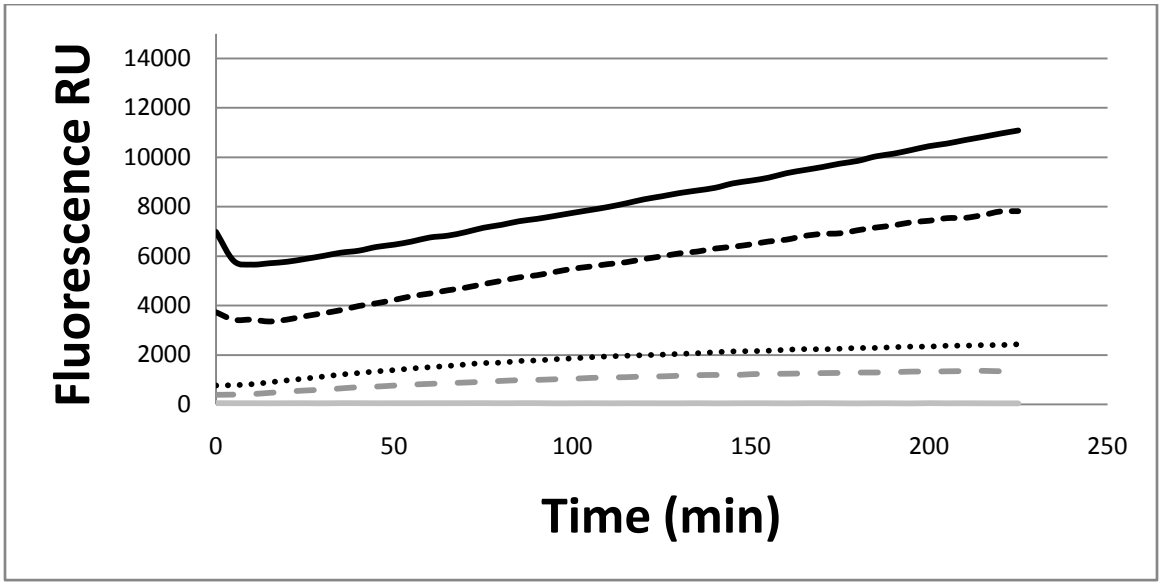

Figure 18-Standard FD8oxoGC assay with 20 ug Jurkat extracts per reaction at different substrate concentrations: 50 nM (solid gray), 100 nM (dotted black), 500 nM (dashed black), 1 uM (solid black)

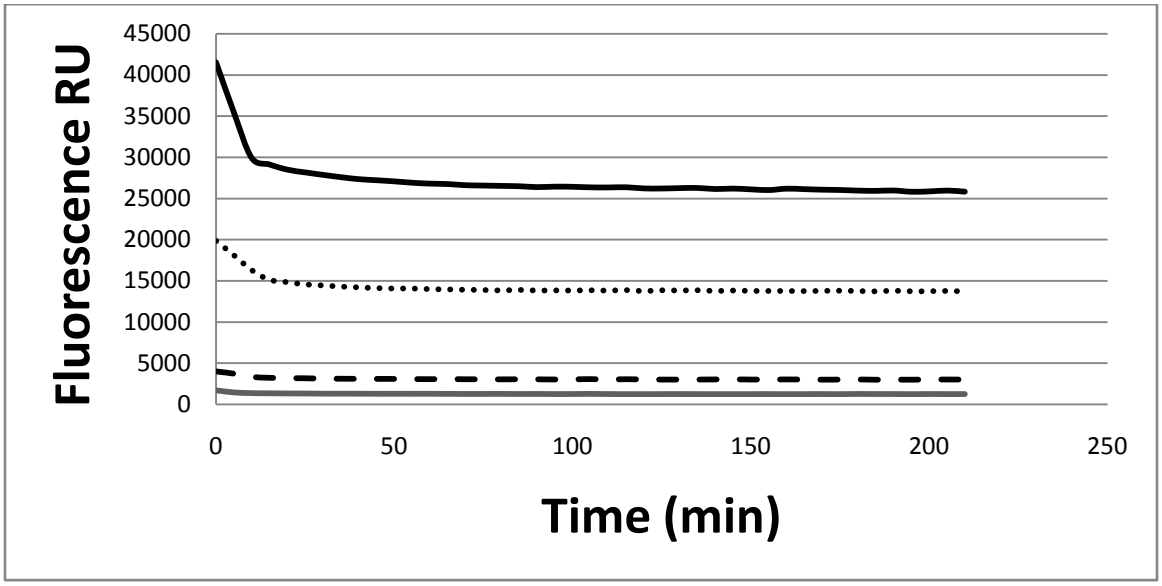

Figure 19-Standard FL35 assay with 20 ug Jurkat extracts per reaction at different substrate concentrations: 50 nM (solid gray), 100 nM (dashed black), 500 nM (dotted black), 1 uM (solid black)

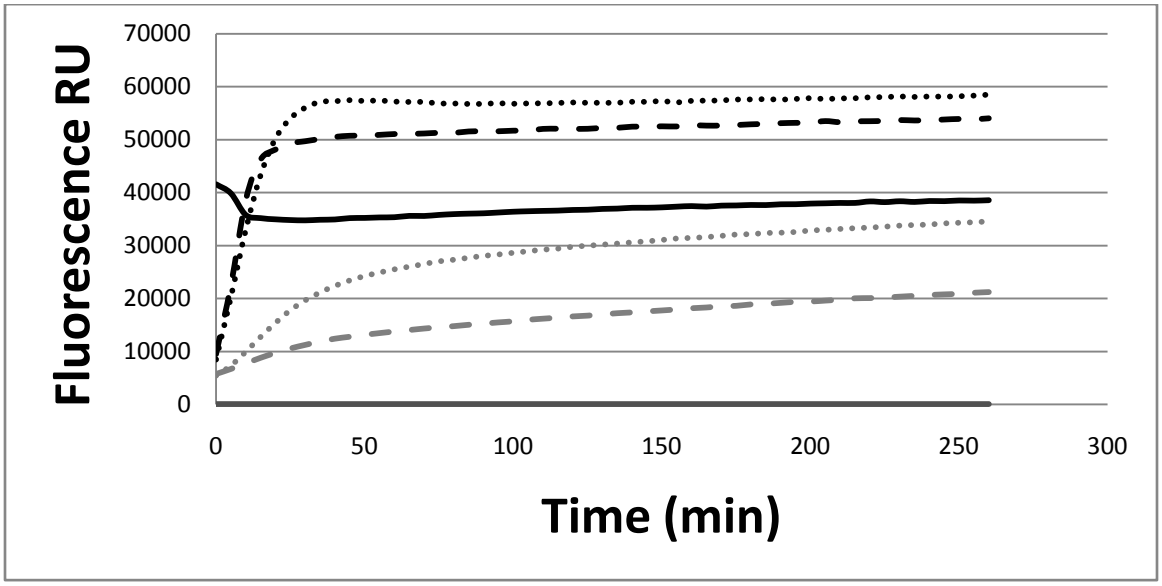

Figure 20- 500 nM of each MB incubated with 30 ug Jurkat extracts. Buffer only (solid gray),FL35 (solid black), FD35 (dashed gray), FDU (dashed black), FDAPE1 (dotted black), FD8oxoGC (dotted gray).

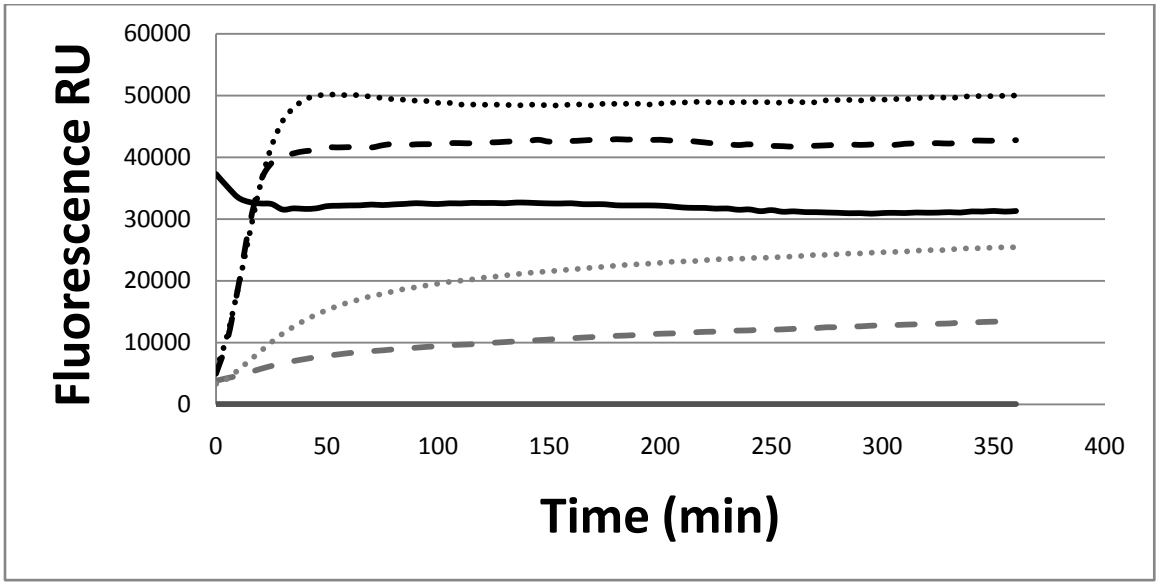

Figure 21-1.25 mM of each MB incubated with 30 ug Jurkat extracts. Buffer only (solid gray),FL35 (solid black), FD35 (dashed gray), FDU (dashed black), FDAPE1 (dotted black), FD8oxoGC (dotted gray).

D. Kinetic Parameter Estimation

k-Value

The fluorescence data gathered from each of the MB at varying concentrations can be fit to a simple saturation curve as described in Equation 1. Nonlinear regression was performed using the lsqcurvefit function in MATLAB. A curve was fitted to each individual MB replicate at every substrate concentration individually. The FDU and FDAPE1 raw fluorescence and time data were directly input into the function and a least squares approach was used to estimate the A_0, saturation value, and the k, rate constant. A similar model was described previously (Leipold, Workman et al. 2003; Krishnamurthy, Zhao et al. 2008). For the FD8oxoGC which had a much lower rate of fluorescence increase, the FD35 quadruplicates were averaged at each time point and subtracted from the FD8oxoGC fluorescence data. This was necessary because in the time

frame of the experiment, FDU and FDAPE1 reached their maximum fluorescence values, the FD8oxoGC did not, and thus was increasing due to both the nonspecific nucleases and Ogg1 and APE1. Previously, it had been shown that whole cell extracts do not repair 8oxoG with a high efficiency which the obtained results also suggest this (Cappelli, Degan et al. 2000).

$$P = A_0\left(1 - e^{-kt}\right)$$

Equation 1-Fit model for base excision repair assay. P = converted product. A0 = Total substrate saturation level in reaction. k = rate constant. t = time.

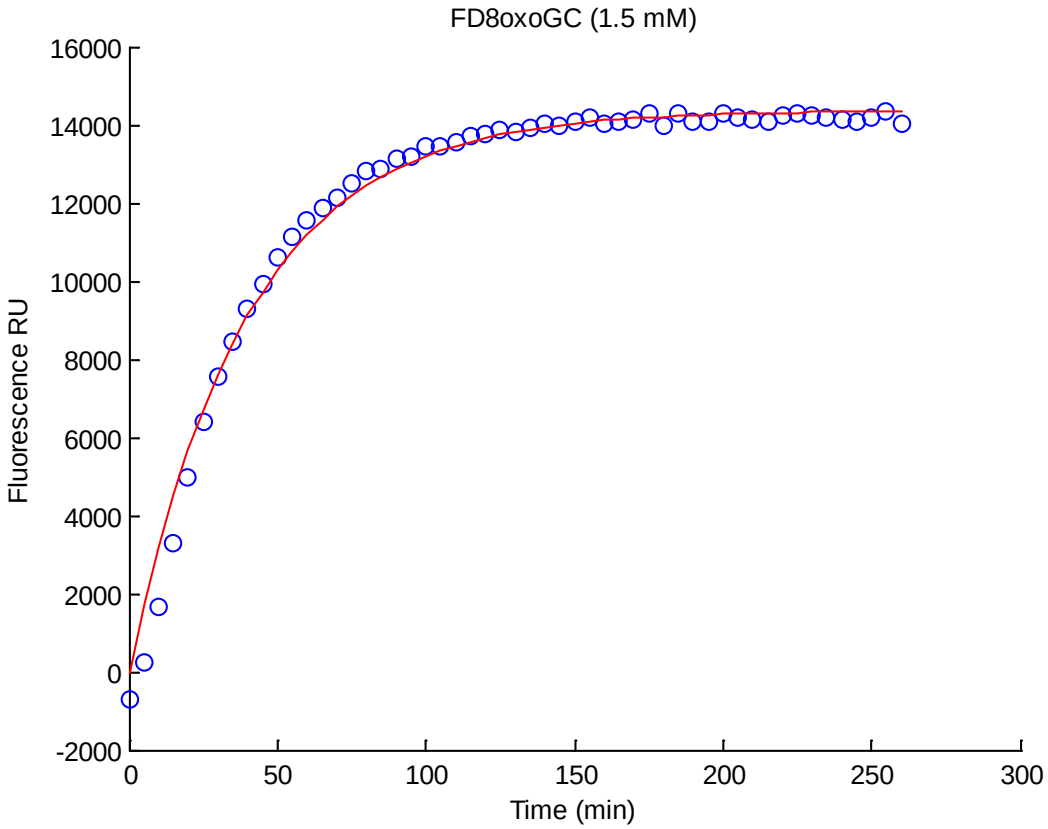

Figure 22-MATLAB generated plot 1.5 mM FD8oxoGC fluorescence data adjusted for FD35 (blue dots) while incubated with 30 ug Jurkat extracts. The red line shows the curve fit using the estimated parameters.

Estimated k-values averages for each of the substrates are shown in Figure 22, Figure 23, and Figure 24. The k-values for each of the substrates at varying concentrations were shown to be substrate concentrations independent with the associated p values all less than 0.05.

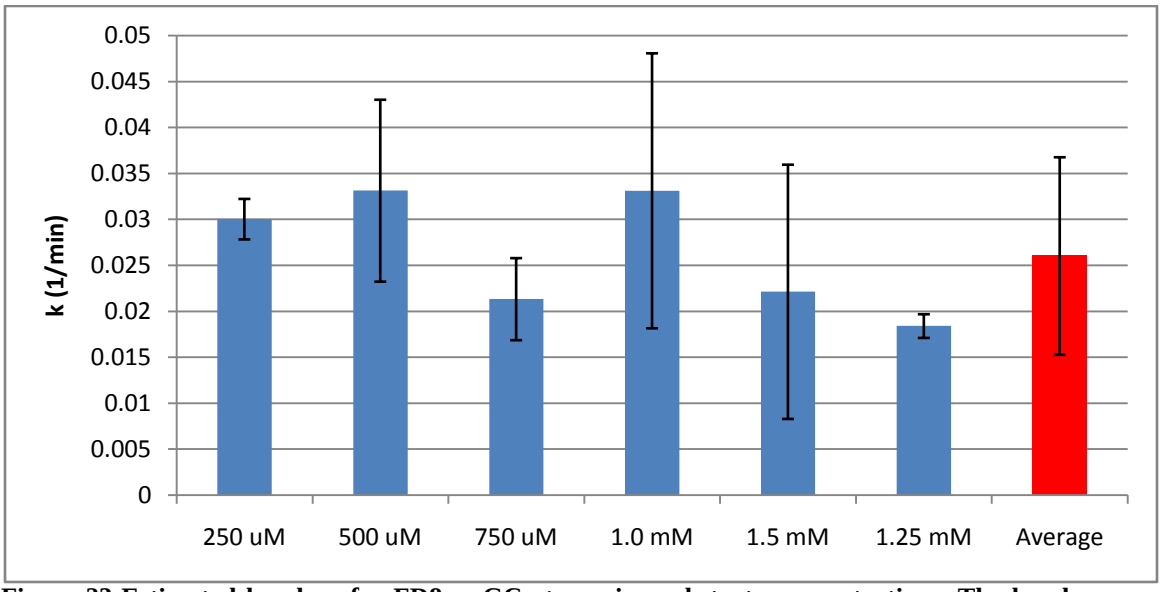

Figure 23-Estimated k-values for FD8oxoGC at varying substrate concentrations. The k-values are substrate independent with a calculated p value of less than 0.05.

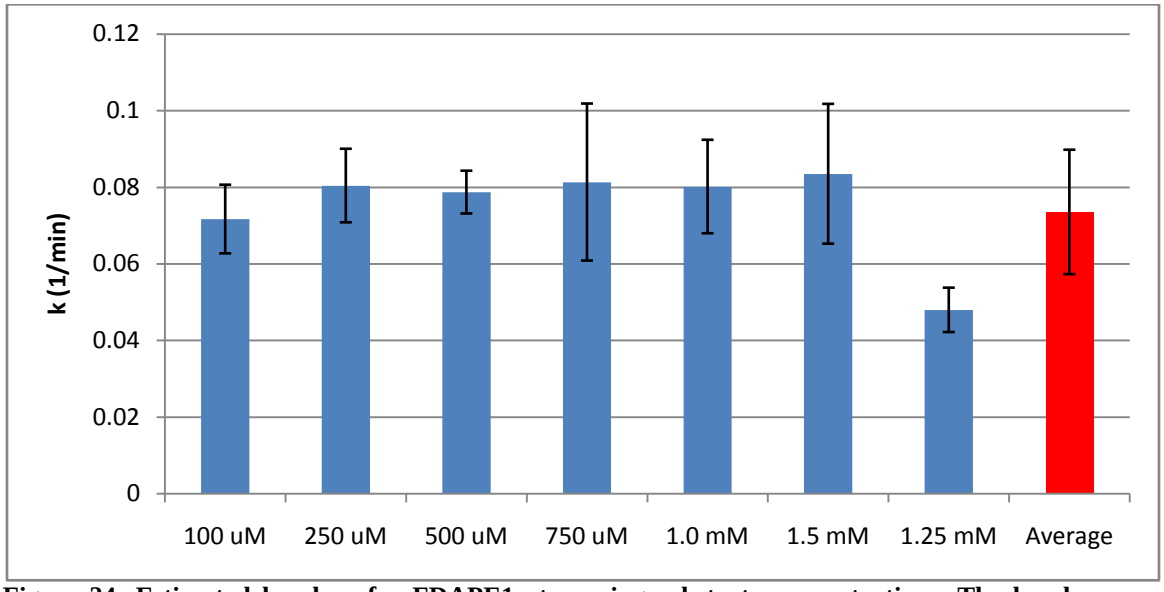

Figure 24- Estimated k-values for FDAPE1 at varying substrate concentrations. The k-values are substrate independent with a calculated p value of less than 0.01.

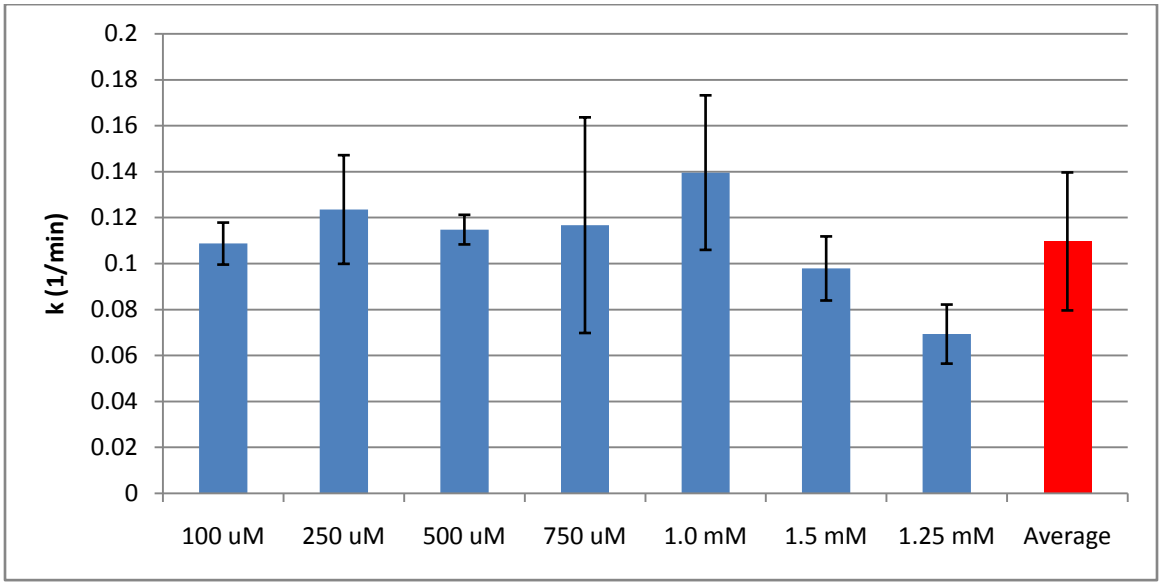

Figure 25- Estimated k-values for FDU at varying substrate concentrations. The k-values are substrate independent with a calculated p value of less than 0.05.

V_{max} and K_m

V_{max} and K_m values were also estimated via lsqcurvefit function in MATLAB from the fluorescence data. For this, initial reaction velocities (V_0) on each of the MBs at each varying concentration were required. Initial velocities were estimated by finding the change in fluorescence over time in the initial linear region of the fluorescence curve. Equation 2 shows how the fluorescence raw data that had been optimized to a positive control regardless of substrate concentration was transformed to obtain an initial velocity in terms of substrate concentration per unit time. In MATLAB, the lsqcurvefit function was used to fit the Michaelis-Menten enzyme kinetics equation to the initial velocities and substrate concentration data input. For this estimation, quadruplicates existed for each substrate concentration used for fitting the curve.

$$V_0 = \left(\frac{\Delta Fluorescence}{\Delta t}\right)\left(\frac{Initial\ Substrate\ Concentration}{A_0}\right)$$

Equation 2-Transformation of fluorescence raw data into substrate concentration using the estimated saturation value (A0) to have an initial velocity in terms of a substrate concentration per unit time.

$$V_0 = V_{max}\left(\frac{[S]}{K_m + [S]}\right)$$

Equation 3-Michaelis-Menten enzyme kinetics equation V_0 (initial velocity), [S] (substrate concentration), V_{max} (maximum initial velocity), and K_m (concentration at which 1/2 maximum velocity is observed.

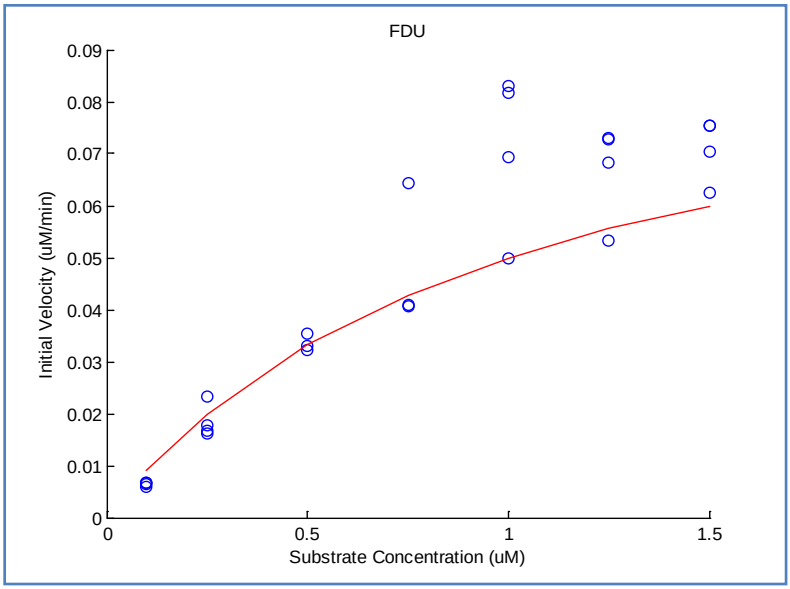

Figure 26- MATLAB plot of FDU initial velocities (blue dots) at varying substrate concentrations to fit a Michaelis-Menten enzyme kinetic model. The red line shows the curve generated using the estimated kinetic parameters.

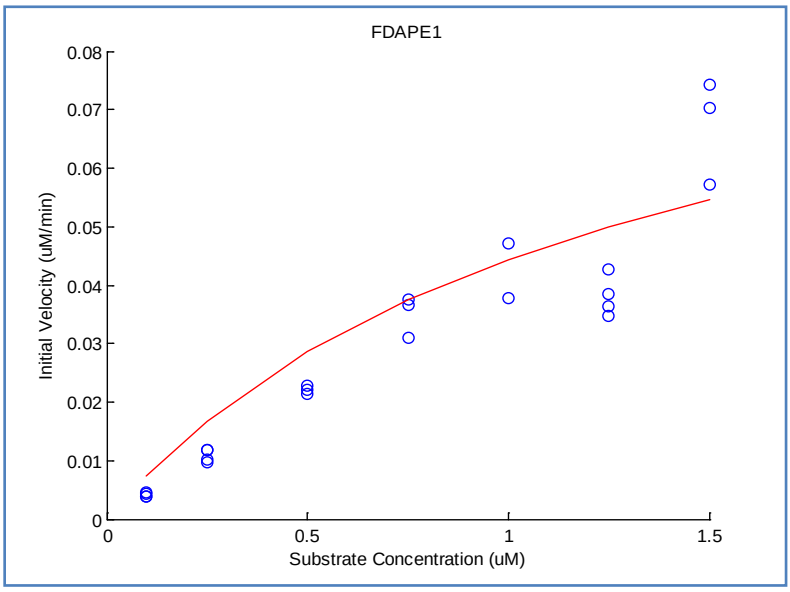

Figure 27- MATLAB plot of FDAPE1 initial velocities (blue dots) at varying substrate concentrations to fit a Michaelis-Menten enzyme kinetic model. The red line shows the curve generated using the estimated kinetic parameters.

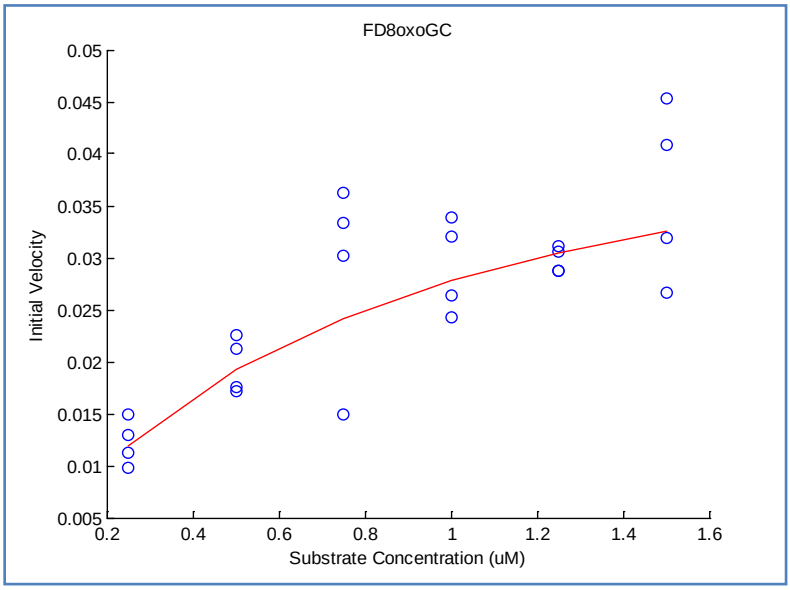

Figure 28- MATLAB plot of FD8oxoGC initial velocities (blue dots) at varying substrate concentrations to fit a Michaelis-Menten enzyme kinetic model. The red line shows the curve generated using the estimated kinetic parameters.

Table 3-Estimated kinetic parameters fit to the Michaelis-Menten model and the associated R^2 values.

Substrate	Vmax (min^{-1})	Km (uM)	R^2
FD8oxoGC	0.053	0.794	0.5105
FDAPE1	0.83	19.74	0.8732
FDU	0.155	1.594	0.8502

V. Conclusions

A simple, reproducible, and versatile base excision assay has been described and validated for potential use in many applications. The protocol described has been optimized for the enzymes involved in 8oxoG and uracil removal but can be easily modified for other types of damage. Nonspecific nuclease activity remains the main challenge of using this type of technology, but the addition of EDTA has been shown to effectively suppress nonspecific activity. Although EDTA seems to decrease the activity of the targeted proteins, specifically APE1, addition of magnesium ions restores the activity. The assay also has been shown to be reproducible for base excision enzymes with both high and low base removal efficiencies. By merely subtracting the nonspecific activities from low efficiency proteins, the activity of slower removal can be easily obtained.

The FRET-based molecular beacons described can be easily modified to include other damaged bases for analysis of other base excision proteins. This technology also has the possibility of being used for a full *in vitro* base excision repair model. Optimizing conditions for enzymes required for nicking of the strand is critical in substrates with single damages. Also, the assay can be used on different types of cell lysates. The estimated kinetic parameters can be used to describe base excision efficiency in different populations(Sokhansanj and Wilson 2006). The efficiency changes due to protein variants can also be assayed using this protocol. Also, base excision repair has been linked to both aging and disease and this assay can be used to possibly further validate those associations (Gensler and Bernstein 1981; Wilson and Bohr 2007). Previously, it has been shown that these molecular beacons can be transfected into cells(Maksimenko, Ishchenko et al. 2004).

VI. References

Boiteux, S. and J. P. Radicella (2000). "The human OGG1 gene: structure, functions, and its implication in the process of carcinogenesis." Archives of Biochemistry and Biophysics **377**(1): 1-8.

Cappelli, E., P. Degan, et al. (2000). "Comparative repair of the endogenous lesions 8-oxo-7, 8-dihydroguanine (8-oxoG), uracil and abasic site by mammalian cell extracts: 8-oxoG is poorly repaired by human cell extracts." Carcinogenesis **21**(6): 1135-1141.

David, S. S., V. L. O'Shea, et al. (2007). "Base-excision repair of oxidative DNA damage." Nature **447**(7147): 941-950.

Gensler, H. L. and H. Bernstein (1981). "DNA damage as the primary cause of aging." The Quarterly review of biology **56**(3): 279-303.

Hegde, M. L., T. K. Hazra, et al. (2008). "Early steps in the DNA base excision/single-strand interruption repair pathway in mammalian cells." Cell research **18**(1): 27-47.

Hill, J. W., T. K. Hazra, et al. (2001). "Stimulation of human 8-oxoguanine-DNA glycosylase by AP-endonuclease: potential coordination of the initial steps in base excision repair." Nucleic acids research **29**(2): 430-438.

Ischenko, A. A. and M. K. Saparbaev (2002). "Alternative nucleotide incision repair pathway for oxidative DNA damage." Nature **415**(6868): 183-187.

Kreklau, E. L., M. Limp-Foster, et al. (2001). "A novel fluorometric oligonucleotide assay to measure O(6)-methylguanine DNA methyltransferase, methylpurine DNA glycosylase, 8-oxoguanine DNA glycosylase and abasic endonuclease activities: DNA repair status in human breast carcinoma cells overexpressing methylpurine DNA glycosylase." Nucleic Acids Res **29**(12): 2558-66.

Krishnamurthy, N., X. Zhao, et al. (2008). "Superior removal of hydantoin lesions relative to other oxidized bases by the human DNA glycosylase hNEIL1." Biochemistry **47**(27): 7137-46.

Krokan, H. and C. U. Wittwer (1981). "Uracil DNa-glycosylase from HeLa cells: general properties, substrate specificity and effect of uracil analogs." Nucleic Acids Res **9**(11): 2599-613.

Leipold, M. D., H. Workman, et al. (2003). "Recognition and removal of oxidized guanines in duplex DNA by the base excision repair enzymes hOGG1, yOGG1, and yOGG2." Biochemistry **42**(38): 11373-81.

Liu, B., X. Yang, et al. (2007). "Real-time monitoring of uracil removal by uracil-DNA glycosylase using fluorescent resonance energy transfer probes." Anal Biochem **366**(2): 237-43.

Maksimenko, A., A. A. Ishchenko, et al. (2004). "A molecular beacon assay for measuring base excision repair activities." Biochem Biophys Res Commun **319**(1): 240-6.

Malins, D. C., N. L. Polissar, et al. (2000). "Single 8-oxo-guanine and 8-oxo-adenine lesions induce marked changes in the backbone structure of a 25-base DNA strand." Proceedings of the National Academy of Sciences of the United States of America **97**(23): 12442-12445.

Nyborg, J. K. and O. B. Peersen (2004). "That zincing feeling: the effects of EDTA on the behaviour of zinc-binding transcriptional regulators." Biochem J **381**(Pt 3): e3-4.

Paz-Elizur, T., D. Elinger, et al. (2007). "Development of an enzymatic DNA repair assay for molecular epidemiology studies: distribution of OGG activity in healthy individuals." DNA Repair (Amst) **6**(1): 45-60.

Sidorenko, V. S., G. A. Nevinsky, et al. (2007). "Mechanism of interaction between human 8-oxoguanine-DNA glycosylase and AP endonuclease." DNA repair **6**(3): 317-328.

Smeaton, M. B., P. S. Miller, et al. (2007). "Small-scale extracts for the study of nucleotide excision repair and non-homologous end joining." Nucleic Acids Res **35**(22): e152.

Sokhansanj, B. A. and D. M. Wilson, 3rd (2006). "Estimating the effect of human base excision repair protein variants on the repair of oxidative DNA base damage." Cancer epidemiology, biomarkers & prevention : a publication of the American Association for Cancer Research, cosponsored by the American Society of Preventive Oncology **15**(5): 1000-1008.

Strauss, P. R., W. A. Beard, et al. (1997). "Substrate binding by human apurinic/apyrimidinic endonuclease indicates a Briggs-Haldane mechanism." J Biol Chem **272**(2): 1302-7.

Tchou, J., H. Kasai, et al. (1991). "8-oxoguanine (8-hydroxyguanine) DNA glycosylase and its substrate specificity." Proc Natl Acad Sci U S A **88**(11): 4690-4.

Vidal, A. E., I. D. Hickson, et al. (2001). "Mechanism of stimulation of the DNA glycosylase activity of hOGG1 by the major human AP endonuclease: bypass of the AP lyase activity step." Nucleic acids research **29**(6): 1285-1292.

Wilson, D. M., 3rd and V. A. Bohr (2007). "The mechanics of base excision repair, and its relationship to aging and disease." DNA repair **6**(4): 544-559.

VII. Appendix

Table 4-Estimated Parameters for FD8oxoGC

[S] (uM)	A_0 (fluor)	k (min^{-1})	R^2
0.25	10907.38	0.028477	0.960067
0.25	10060.83	0.031591	0.978218
0.5	14365.73	0.025154	0.959856
0.5	14187.14	0.023995	0.990451
0.5	11630.25	0.041908	0.998911
0.5	13743.62	0.041466	0.999032
0.75	7990.356	0.027207	0.994493
0.75	18070.49	0.022253	0.980423
0.75	7626.782	0.018761	0.997729
0.75	6043.426	0.01712	0.995469
1	15410.18	0.020306	0.997179
1	17267.1	0.053652	0.968543
1	12697.91	0.034503	0.997929
1	11538.32	0.024007	0.998202
1.5	11974.91	0.030052	0.984889
1.5	12609.77	0.037423	0.973828
1.5	10930.1	0.008581	0.998961
1.5	11331.03	0.012475	0.999306
1.25	11681.75	0.016917	0.990591
1.25	12362.33	0.017755	0.997112
1.25	12101.1	0.019327	0.998403
1.25	11446.74	0.019626	0.998808

Table 5- Estimated Parameters for FDAPE1

[S] (uM)	A_0 (fluor)	k (min^{-1})	C (fluor)	R^2
0.1	42534.024	0.0803218	6291.4304	0.9865469
0.1	38569.514	0.0615426	4996.4293	0.9968408
0.1	42809.758	0.0780041	5885.321	0.9852882
0.1	43551.443	0.0668466	5483.2303	0.9867476
0.25	36314.089	8.77E-02	4843.4947	0.9849005
0.25	52089.876	0.0726455	4824.8007	0.9835739

0.25	53981.377	0.0716417	4192.2241	0.9758786
0.25	48837.248	0.0896523	4336.5264	0.9742323
0.5	52404.674	0.0740835	5505.1618	0.991817
0.5	56011.189	8.49E-02	5918.763	0.9877539
0.5	50918.999	0.0771426	7160.4613	0.9899089
0.75	51462.536	7.20E-02	4.81E+03	0.9849224
0.75	57381.53	6.72E-02	5.01E+03	0.9809221
0.75	54402.289	0.1048383	7451.914	0.9880185
1	56674.873	0.0887925	6332.1749	0.9977076
1	52296.042	0.0715407	2377.1881	0.9880676
1.5	50228.763	0.0880375	5356.3848	0.9816769
1.5	44574.013	0.0634121	3059.0333	0.9977131
1.5	40877.114	0.099037	4759.2012	0.9976125
1.25	51925.93	0.042321	1815.8204	0.9821958
1.25	50687.511	0.0456214	2413.6986	0.9819049
1.25	51265.379	0.0480361	1675.185	0.9770601
1.25	60823.108	0.055922	2388.0275	0.974293

Table 6- Estimated Parameters for FDU

[S] (uM)	A_0 (fluor)	k (min^{-1})	C (fluor)	R^2	[S] (uM)
0.1	31396.17	0.104722	8049.1	1.91E+09	0.998751
0.1	39460.84	0.12001	9423.518	2.79E+09	0.992506
0.1	33860.07	0.098725	8878.751	1.78E+09	0.994385
0.1	30880.31	0.111403	7160.788	1.64E+09	0.998469
0.25	31356.56	0.158149	7052.269	1.63E+09	0.973604
0.25	30003.93	0.113011	5017.803	1.29E+09	0.993735
0.25	37111.18	0.105273	5669.094	2.58E+09	0.995919
0.25	49110.16	0.117724	8916.314	9.01E+09	0.998297
0.5	44064.28	0.120099	6931.416	2.67E+09	0.990171
0.5	41783.11	0.10763	8532.471	2.82E+09	0.988495
0.5	44563.58	0.116641	8198.371	3.43E+09	0.987352
0.75	40951.49	0.092222	3729.412	2.02E+09	0.978712
0.75	39928.02	0.087148	4241.519	2E+09	0.981583
0.75	41068.38	0.170809	7201.699	3.49E+09	0.98356

1	48511.7	0.167233	7723.59	3.11E+09	0.921
1	43112.94	0.155567	7263.968	2.55E+09	0.984012
1	43665.89	0.144433	5854.052	2.34E+09	0.910701
1	41220.82	0.091138	3770.112	1.87E+09	0.972454
1.5	44852.67	0.093084	3747.204	2.39E+09	0.977711
1.5	35653.59	0.108413	3517.633	1.52E+09	0.969349
1.5	38080.41	0.080327	2161.945	1.43E+09	0.957508
1.5	36002.84	0.109758	3296.302	1.54E+09	0.968388
1.25	46097.08	0.050249	1334.808	2.33E+09	0.980773
1.25	40546.9	0.0736	2286.409	1.91E+09	0.964736
1.25	40661.73	0.075675	1870.45	1.91E+09	0.961868
1.25	41021.68	0.077863	2252.694	1.96E+09	0.96272